Study of isomeric states in ^{198,200,202,206}Pb and ^{206}Hg populated in fragmentation reactions

Lalović, Nataša; Rudolph, Dirk; Podolyák, Zsolt; Sarmiento Pico, Luis; Simpson, E.C.; Alexander, T.; Cortés, M.L.; Gerl, J.; Golubev, Pavel; Ameil, F.; Arici, T.; Bauer, Ch.; Bazzacco, D.; Bentley, M. A. ; Boutachkov, P.; Bowry, M.; Fahlander, Claes; Gadea, A.; Gellanki, Jnaneswari; Givechev, A.; Goel, N.; Gorska, M.; Gottardo, A.; Gregor, E.; Guastalla, G.; Habermann, T.; Hackstein, M.; Jungclaus, A.; Kojouharov, I.; Kumar, R.; Kurz, N.; Lettmann, M.; Lizarazo, C.; Louchart, C.; Merchán, E.; Michelagnoli, C.; Moeller, Th.; Moschner, K.; Patel, Z.; Pietralla, N.; Pietri, S.; Ralet, D.; Reese, M.; Regan, P.H.; Reiter, P.; Schaffner, H.; Singh, P.; Stahl, C.; Stegmann, R.; Stezowski, O.

Published in:
Journal of Physics G: Nuclear and Particle Physics

DOI:
10.1088/1361-6471/aaa9df

2018

Document Version:
Early version, also known as pre-print

Study of Isomeric States in ^{198,200,202,206}Pb and ^{206}Hg Populated in Fragmentation Reactions

N Lalović[1,2], D Rudolph[1], Zs Podolyák[3], L G Sarmiento[1], E C Simpson[4], T Alexander[3], M L Cortés[5,2]‡, J Gerl[2], P Golubev[1], F Ameil[2], T Arici[6,2], Ch Bauer[5], D Bazzacco[7], M A Bentley[8], P Boutachkov[5], M Bowry[3]§, C Fahlander[1], A Gadea[9], J Gellanki[1]‖, A Givechev[5], N Goel[2], M Górska[2], A Gottardo[7], E Gregor[2], G Guastalla[5,2], T Habermann[2], M Hackstein[10], A Jungclaus[11], I Kojouharov[2], R Kumar[12], N Kurz[2], M Lettmann[5], C Lizarazo[5,2], C Louchart[13], E Merchán[5,2], C Michelagnoli[7]¶, Th Moeller[5], K Moschner[10], Z Patel[3], N Pietralla[5], S Pietri[2], D Ralet[5,2+], M Reese[5], P H Regan[3,14], P Reiter[10], H Schaffner[2], P Singh[5,2], C Stahl[5], R Stegmann[5], O Stezowski[15], J Taprogge[11], P Thöle[10], A Wendt[10], O Wieland[16], E Wilson[3], R Wood[3], H-J Wollersheim[2], B Birkenbach[10], B Bruyneel[13], I Burrows[17], E Clément[18], P Désesquelles[19], C Domingo-Pardo[9], J Eberth[10], V Gonzáles[20], H Hess[10], J Jolie[10], D S Judson[21], R Menegazzo[7], D Mengoni[7,22], D R Napoli[23], A Pullia[24,16], B Quintana[25], G Rainovski[26], M D Salsac[13], E Sanchis[20], J Simpson[17], J J Valiente Dóbon[23] and the AGATA Collaboration

[1]Department of Physics, Lund University, S-22100 Lund, Sweden
[2]GSI Helmholtzzentrum für Schwerionenforschung, D-64291 Darmstadt, Germany
[3]Department of Physics, University of Surrey, Guildford, GU2 XH, United Kingdom
[4]Department of Nuclear Physics, Research School of Physics and Engineering, The Australian National University, Canberra ACT 2612, Australia
[5]Institut für Kernphysik, Technische Universität Darmstadt, D-64289 Darmstadt, Germany
[6]Justus-Liebig-Universität Giessen, D-35392 Giessen, Germany
[7]INFN Sezione di Padova, I-35131 Padova, Italy

‡ Present address: RIKEN Nishina Center, Wako, Saitama, Japan
§ Present address: National Superconducting Cyclotron Laboratory, Michigan State University, East Lansing, Michigan 48824, USA
‖ Present address: Department of Physics and Astrophysics, University of Delhi, Delhi 110007, India
¶ Present address: Institut Laue-Langevin, B.P. 156, F-38042 Grenoble Cedex 9, France
+ Present address: CSNSM, Univ. Paris-Sud, CNRS/IN2P3, Université Paris-Saclay, F-91405 Orsay, France

[8]Department of Physics, University of York, Heslington, York YO10 5DD, United Kingdom
[9]Instituto de Fisica Corpuscular, CSIC-Universitat de Valencia, E-46920 Valencia, Spain
[10]Institut für Kernphysik, Universität zu Köln, D-50937 Köln, Germany
[11]Instituto de Estructura de la Materia, CSIC, E-28006 Madrid, Spain
[12]Inter-University Accelerator Centre, New Delhi 110067, India
[13]CEA, Centre de Saclay, IRFU/Service de Physique Nuclaire, F-91191 Gif-sur-Yvette, France
[14]National Physical Laboratory, Teddington Middlesex, TW11 0LW, UK
[15]Université de Lyon, CNRS-IN2P3, Institut de Physique Nuclaire de Lyon, F-69622 Villeurbanne, France
[16]INFN Sezione di Milano, I-20133 Milano, Italy
[17]STFC Daresbury Laboratory, Daresbury, Warrington, WA4 4AD, United Kingdom
[18]GANIL, CEA/DSAM and CNRS/IN2P3, F-14076 CAEN Cedex 05, France
[19]Centre de Spectrométrie Nucléaire et de Spectrométrie de Masse - CSNSM, CNRS/IN2P3 and Univ. Paris-Sud, F-91405 Orsay Campus, France
[20]Departamento de Ingeniería Electrónica, Universitat de Valencia, Burjassot, E-46100 Valencia, Spain
[21]Oliver Lodge Laboratory, The University of Liverpool, Liverpool, L69 7ZE, United Kingdom
[22]Dipartimento di Fisica e Astronomia dell'Universitá di Padova, I-35131 Padova, Italy
[23]Laboratori Nazionali di Legnaro, INFN, I-35020 Legnaro (PD), Italy
[24]Dipartimento di Fisica dell'Universitá degli Studi di Milano, I-20133 Milano, Italy
[25]Universidad de Salamanca, E-37008 Salamanca, Spain
[26]Faculty of Physics, St. Kliment Ohridski University of Sofia, 1164 Sofia, Bulgaria

E-mail: `Natasa.Lalovic@nuclear.lu.se`

Abstract. Isomeric states in isotopes in the vicinity of doubly-magic ^{208}Pb were populated following reactions of a relativistic ^{208}Pb primary beam impinging on a ^{9}Be fragmentation target. Secondary beams of ^{198,200,202,206}Pb and ^{206}Hg were isotopically separated and implanted in a passive stopper positioned in the focal plane of the GSI Fragment Separator. Delayed γ rays were detected with the Advanced GAmma Tracking Array (AGATA). Decay schemes were re-evaluated and interpreted with shell-model calculations. The momentum-dependent population of isomeric states in the two-nucleon hole nuclei ^{206}Pb/^{206}Hg was found to differ from the population of multi neutron-hole isomeric states in ^{198,200,202}Pb.

PACS numbers: 29.30.Kv, 25.70.Mn, 24.50.+g, 23.20.-g, 21.60.Cs, 27.80.+w

Submitted to: *J. Phys. G: Nucl. Part. Phys.*
Keywords: Gamma-ray spectroscopy, relativistic projectile fragmentation, direct reactions, isomeric decays, electromagnetic transitions, nuclear shell model.

1. Introduction

Isomeric states in nuclei continue to be valuable experimental sources for probing nuclear structure models at or beyond the line of β stability [1]. The abundance of isomeric states is usually high near the doubly-magic cornerstones of the nuclidic chart. In such cases, they are of specific relevance for probing nuclear interactions within the framework of the spherical shell model, since their origin often relates to spin-aligned couplings of a limited number of unpaired particles just above, or unpaired holes just below a filled proton and/or neutron shell. The residual interactions lead to reduced phase space for electromagnetic decay, be it in terms of decay energy or spin difference between initial and final state. The consequence are delayed electromagnetic decays, mostly observed via delayed γ-ray cascades.

For the majority of cases, and in particular those far away from the line of β stability, the preparation of pure isotopic samples is highly beneficial. Starting in the late 1990's (see, e.g., Refs. [2–4]), secondary beams from fragmentation facilities, which provide event-by-event isotopic identification, were combined with increasingly efficient γ-ray detector arrays. A prime example was the *Rare Isotope Spectroscopic INvestigations at GSI* (RISING) campaign: The combination of primary beam energies up to $E/A = 1$ GeV, the GSI Fragment Separator (FRS) [5], and the RISING germanium-detector array [6, 7] gave rise to numerous exciting discoveries of isomeric states near heavy doubly-magic nuclides (see, for example, Refs. [8–10]), including the heaviest known one, namely ^{208}Pb (see, for instance, Refs. [11, 12]). More recently, the RISING scheme was successfully re-established with the EUroball-RIKEN Cluster Array (EURICA) array behind the Big-RIPS separator at RIBF, RIKEN, Japan [13,14].

Besides plain observation of isomeric states by means of γ-ray spectroscopy, their population via a number of possible reaction mechanisms turned into a research subject in its own right (see, e.g. [15, 16]). This includes persistence of spin alignment throughout the reaction and separation stages [17] as well as the possibility for nuclear g-factor measurements (see, e.g., Ref. [18]). The most recent highlight invokes reaction paths via the nucleonic Δ-resonance to explain the observed number of nuclei populated in a given isomeric state (the 'isomeric ratio') and their momentum dependence [19]. In general, isomeric states in few-nucleon hole nuclei, such as ^{206}Pb or ^{206}Hg, provide the hitherto best probes to be addressed by theoretical nuclear reaction models for isomer production [20, 21].

The present study was conducted within the framework of the PreSPEC-AGATA 2012 campaign at GSI [22]. It focuses on both electromagnetic decay sequences and (different) population mechanisms of isomeric states in multi neutron-hole residues ^{198,200,202}Pb, in contrast to isomeric states produced in the two-nucleon hole pair ^{206}Pb/^{206}Hg. The experimental details are provided in Sec. 2, and the experimental results presented in Sec. 3. Section 4 sees both the shell-model interpretation of the spectroscopic results, thereby probing several shell-model parametrizations, and a theoretical assessment of the observed isomeric ratios. The article concludes with a brief summary.

2. Experimental approach

The present study relies on the correlation of γ radiation from isomeric states with a given isotope, using a method which has been proven to be very effective and to provide clean spectroscopic conditions even for heavy nuclei (see, for instance, Refs. [11, 12]).

This is achieved via the production of rare isotopes by fragmentation reactions followed by separation, event-by-event identification, and implantation of the residues in the centre of a Ge-detector array.

The experiment builds upon a ^{208}Pb heavy-ion beam accelerated to 1 GeV/u by the UNILAC-SIS accelerator complex at the GSI Helmholtzzentrum für Schwerionenforschung at Darmstadt, Germany. The primary beam impinged on a 2.5 g/cm^2 ^{9}Be target plus a 0.22 g/cm^2 Nb stripper foil at the entrance of the FRS [5]. The isotopes of interest, namely ^{198,200,202,206}Pb [23] and ^{206}Hg [24,25], are populated by few-nucleon knockout or fragmentation reactions. For each isotope, primary beam intensities and spill lengths were adjusted to match the rate capabilities of the FRS detectors and the PreSPEC-AGATA data-acquisition system, ranging from $6 \cdot 10^7$ ^{208}Pb particles per 10-s spill for ^{206}Pb ions at the beginning of the experiment to $1.2 \cdot 10^9$ particles per 4-s spill for ^{206}Hg or ^{198}Pb toward the end of the experiment.

Following an established calibration procedure (see, for instance, Ref. [26]) of the standard ion identification detectors of the FRS with a low-intensity primary beam, FRS magnet settings for the various isotopes of interest were checked and optimized one by one. The secondary beams had energies of about 830 MeV/u after the primary target and stripper foil. They were slowed down to 380 MeV/u at the middle focal plane of the FRS, mainly due to a 5-6 g/cm^2, wedge-shaped Al degrader. Finally, all secondary beams were set to reach the secondary target and stopper located at the FRS final focus, S4, with 160 MeV/u.

Since ions of interest are close in mass, A, and proton number, Z, to the primary beam, the high production cross-sections allowed the high beam purity of various secondary beams. It is predicted and measured to be rather high at S4, ranging from about 90% for ^{198}Pb up to some 98% for ^{206}Pb, for the different FRS settings. In turn, H-like and He-like primary beam particles needed to be suppressed by slits in x direction perpendicular to the beam direction at the first, S1, and intermediate, S2, FRS focal plane, respectively. These slits are mandatory to keep the particle rate for the tracking and time-of-flight start detectors at S2 manageable. Their placement at S1 and S2 was the same for all Pb isotopes, $\pm$15 mm and $\pm$20 mm, respectively. In the case of ^{206}Hg, the slits were confining $-11 + 8$ mm and $-25 + 38$ mm of the primary beam, in relation to the central trajectory.

At the final focal plane, S4, the standard FRS time-of-flight stop scintillator, two time projection chambers for beam tracking, and two multi-sampling ionization chambers (MUSIC) [27] allow for event-by-event identification of each incoming ion in combination with signals from the detectors at S2. The ions then enter the PreSPEC-AGATA secondary target vacuum chamber. This chamber comprises a LYCCA [32] time-of-flight scintillator, a 32-strip by 32-strip, 0.31 mm thick LYCCA double-sided Si strip detector (target DSSSD) and secondary target ladders at the nominal 23.5 cm distance and a close target position (15 cm downstream) with respect to the γ-ray spectrometer AGATA [28]. For the isomer data discussed here, a 10-mm thick piece of plastic was used at the close position to stop the secondary ions. For in-beam experiments following the isomer runs, the plastic stopper was removed, and a 400 mg/cm^2 gold foil placed at the nominal target position, with tertiary ions identified and stopped in the LYCCA wall [32] some 3 m downstream from the PreSPEC-AGATA chamber [29]. Note, however, that detailed numerical knowledge on isomeric ratios is a mandatory prerequisite for any subsequent derivation of reduced transition probabilities, $B(E2; 2+ \rightarrow 0^+)$, from Coulomb excitation.

The AGATA sub-array, installed at GSI at the beginning of the PreSPEC

campaign, encompassed 17 electrically segmented HPGe crystals. The digital energy threshold for recording γ-ray data was put as low as possible to not trigger the noise, $\sim 20-50$ keV depending on the crystal. Data acquisition trigger for measurement of isomers requested only a particle detected in the last plastic scintillator of the FRS [30]. The rate of validated triggers was in the range from 1.0 kHz to 1.9 kHz. Thereafter, data was recorded by means of two individual data acquisition systems for FRS (and LYCCA) as well as AGATA [28]. Correlation between the two data streams was performed in the offline analysis, merging events with matching timestamps within a 20 μs time window. This yielded an effective, clean time window of 10 μs as an upper limit for the analysis of the delayed decay data [23, 30].

3. Analysis and results

During the offline data processing, raw data from AGATA crystals in form of digitally recorded waveforms were refined by means of energy calibration, cross-talk correction, time alignment and eventual energy compensation for up to two absent segment signals. Details of the corresponding procedures are presented in Refs. [23, 33]. An algorithm demonstrating the underlying principle of AGATA, Pulse Shape Analysis (PSA) [34], is performed already on-line. However, various refinements in data treatment are applied at different stages of the data flow (see, e.g., Ref. [30] and Appendix A in Ref. [31]). Therefore, the PSA is performed offline once more to ensure the validity of corrections applied to the raw data.

The event-by-event ion identification is done by a two-dimensional selection in velocity $\beta = v/\mathrm{c}$, which depends on mass, A, and proton number, Z. The latter is based on the energy-loss measurements in the two MUSICs, *and* affirmed by the energy-loss information from the target DSSSD. This ensures that the number of ions passing this condition equals the number of selected secondary beam particles implanted in the plastic stopper.

The isomeric ratio, R_{exp}, represents the number of nuclei produced in a certain isomeric state out of all nuclei produced in a primary reaction. Isomeric ratios were derived from experimental data using the equation:

$$R_{exp} = \frac{\frac{N_\gamma}{\epsilon_{abs} b_t}(1+\alpha_{tot})}{N_{imp} F} \cdot 100 \tag{1}$$

The numerator is a measure of the effective number of γ-ray decays following the deexcitation of the particular isomeric state. N_γ is determined by the integral of the delayed γ-ray peak, ϵ_{abs} is the absolute efficiency of the AGATA sub-array [31], and b_t is the branching ratio for the observed γ-ray transition. For internal conversion coefficients, α_{tot}, BRICC [35] was consulted. The denominator represents the number of identified ions, N_{imp}, corrected by the factor F, as a property of the experimental set-up. Several individual correction factors, f_1 - f_4, contribute to $F = f_1 \cdot f_2 \cdot f_3 \cdot f_4$:

- f_1 corrects for those time intervals when AGATA is unresponsive to the emitted γ rays due to the prompt radiation [36].
- f_2 corrects for the portion of ions populated in the isomeric state of interest which might decay in flight, i.e. from the production target to the final focal plane.
- f_3 takes into account the exact time limits of the time window for the delayed γ-ray spectra.

- f_4 accounts for the fraction of implanted ions that did not undergo tertiary nuclear reactions in the plastic stopper.

More details of an applied procedure to calculate isomeric ratios are given in Ref. [23].

At the beginning of the correlation analysis, γ-ray spectra were inspected for implanted ^{198,200,202,206}Pb as well as ^{206}Hg nuclei. Different generic ranges for the correlation time period after the implantation have been investigated, focusing on isomeric γ decay in the few-tenths of nanosecond to few-microsecond regimes. In the process of the analysis it was found sufficient to use AGATA in its so-called 'core common' mode [31].

The following subsections summarize the spectroscopic results and derived isomeric ratios isotope by isotope. The numerical results are summarized in Table 1, which lists the observed isomeric states, their main characteristics, and their isomeric ratios.

3.1. Isomeric States in ^{206}*Hg*

There are two previously reported isomeric states [37–39] — an $I^\pi = 10^+$ level with $T_{1/2} = 92(8)$ ns [37, 38] (Steer *et al* measured $T_{1/2} = 112(4)$ ns) and an $I^\pi = 5^-$ level with $T_{1/2} = 2.15(21)$ μs — the decays of which were observed in the current experiment. Previously published values were extracted from a deep-inelastic reaction [38] and a projectile fragmentation experiment [39] similar to the one described here. The former has been experimentally exploited for population of yrast isomeric states, though not being isotopically clean to the same extent as the fragmentation reaction.

After applying software gates to the time-energy correlation matrices, delayed γ-ray spectra for the two states of interest are singled out as displayed in Fig. 1. Different time ranges, addressing different half-lives of the two isomeric states, were used to produce these spectra as energy projections from the time-energy matrix. The quantities relevant for the isomeric-ratio calculation regarding delayed γ data are indicated in Fig. 1: γ transition energies, exact time ranges, and deduced half-lives.

The half-life values from this measurement agree with already published information and amount to $T_{1/2} = 106(15)$ ns for the $I^\pi = 10^+$ and $T_{1/2} = 2.08(4)$ μs for the $I^\pi = 5^-$ state. The two relevant decay curves are shown as insets in Fig. 1. It is important to emphasize that the intention of this study was not a dedicated half-life determination. Thus the experimental conditions were not strictly adjusted for such a measurement. Despite that, the newly obtained values are not only comparable and consistent, but in some cases even reduce the uncertainties with respect to previously published values. This leads to updated adopted weighted average values. For ^{206}Hg, they become $T_{1/2} = 108(6)$ ns for the $I^\pi = 10^+$ isomer and $T_{1/2} = 2.09(3)$ μs for the $I^\pi = 5^-$ isomer. These values are used in the partial level scheme shown in Fig. 2.

Due to the very different half-lives of the two states, the isomeric-ratio determination was not hampered by the fact that the lower-lying isomer is fed by the higher-lying one. As stated in Table 1, the isomeric ratio of the 10^+ state, which amounts to 3.5(2)%, is subtracted from the value for the 5^- state, yielding 29.7(13)% for the latter.

3.2. Isomeric States in ^{206}Pb

In ^{206}Pb two isomeric states [37, 40–42] are known: an $I^\pi = 12^+$ level with $T_{1/2} = 202(3)$ ns and an $I^\pi = 7^-$ level with $T_{1/2} = 125(2)$ μs. They are observed in the present work. As seen in Fig. 3, the half-life for the 12^+ state was the only one determined in this work, $T_{1/2} = 203(28)$ ns. The half-life of the 7^- isomer is too long for the experimental conditions of the present measurement. The new adopted value of the 12^+ state half-life is given in the partial level scheme of ^{206}Pb in Fig. 4. The resulting isomeric ratios are 1.3(2)% and 22.4(16)% for $I^\pi = 12^+$ and $I^\pi = 7^-$, respectively. Note that the value corresponding to the $I^\pi = 7^-$ is obtained by subtracting observed feeding from the $I^\pi = 12^+$ state.

3.3. Isomeric States in ^{202}Pb

In the case of ^{202}Pb, three previously known isomeric states have been studied [43], namely an $I^\pi = 19^-$ with $T_{1/2} = 107(3)$ ns, an $I^\pi = 16^+$ with $T_{1/2} = 110(5)$ ns, and an $I^\pi = 7^-$ with $T_{1/2} = 65.4(2)$ ns. The corresponding partial level scheme is shown in Fig. 6. In addition to these states, another very long-lived isomeric state has previously been published [43, 44] – an $I^\pi = 9^-$ with $T_{1/2} = 3.54(2)$ h. Considering the limited time window for delay measurements described here, γ-ray transition depopulating this 9^- yrast state cannot be observed.

The resulting isomeric ratios are 0.5(1)%, 2.2(3)%, and 9.0(7)% for $I^\pi = 19^-$, $I^\pi = 16^+$ (corrected for observed feeding from the $I^\pi = 19^-$), and $I^\pi = 7^-$, respectively.

The analysis of ^{202}Pb revealed a weak presence of γ transitions originating from ^{200}Pb. To ensure that the identification selection only singles out ions of ^{202}Pb, those weak delayed contaminant lines were separated. They were selected and correlated with entries in the two-dimensional selection they stem from, as described at the beginning of Sec. 3. However, a recognizable pattern in the corresponding β versus Z histogram was missing. Subsequently, subtracting such a histogram from the one before the contaminant removal had no effect on the final γ spectrum displayed in Fig. 5. The seemingly contaminating transitions were thus attributed to residues of tertiary neutron knockout in the stopper [45].

3.4. Isomeric States in ^{200}Pb

Isomeric decays of three previously reported states [41, 44, 47, 50] — an $I^\pi = 19^-$ with $T_{1/2} = 72(3)$ ns, an $I^\pi = 12^+$ with $T_{1/2} = 199(3)$ ns, and an $I^\pi = 9^-$ with $T_{1/2} = 448(12)$ ns — have been analysed. The (9^-) isomer was implicitly observed, due to the fact that it was fed from the states above (see Fig. 8).

The level scheme of ^{200}Pb shown in Fig. 8 suggests that the four isomeric states actually represent a 'decay chain'. Therefore, the half-life analysis of the $I^\pi = (9^-)$ level accounted for the feeding from the decays of preceding isomeric states. Hence, its half-life was extracted using the Bateman equation [46] for four exponential decays of a chain [23]. The resulting value of half-life agrees very well with all individual literature values listed in Ref. [47] except for one value measured by Fant *et al* [44]. We emphasize the irreproducibility of the latter and note that Ref. [44] does not provide a decay curve. Thus this data point was excluded from the weighted average calculation to obtain the new adopted value of $T_{1/2} = 482(11)$ ns. The isomeric ratios determined for the three states are 0.8(2)%, 13.4(8)%, and 19.5(10)% for $I^\pi = 19^-$,

$I^\pi = 12^+$, and $I^\pi = 9^-$, respectively. Similar to the nuclei presented in previous sections, the isomeric ratios of the lower-lying states are corrected for the feeding from the states above.

3.5. Isomeric States in ^{198}Pb

Much as in the case of ^{200}Pb, the level scheme of ^{198}Pb (see Fig. 10) suggests four isomeric states [48,49] in a decay chain. Literature quotes the following values of their corresponding half-lives: $T_{1/2} = 212(4)$ ns for $I^\pi = (12)^+$ level, $T_{1/2} = 137(10)$ ns for $I^\pi = (9)^-$ level, $T_{1/2} = 4.19(10)$ μs for $I^\pi = (7)^-$ level, and $T_{1/2} = 50.4(5)$ ns for $I^\pi = (5)^-$ level. We have measured half-lives of $I^\pi = (12)^+$ level with $T_{1/2} = 212(5)$ ns and $I^\pi = (7)^-$ with $T_{1/2} = 4.12(10)$ μs (see Fig. 9). The latter is a result of the fitting routine incorporating four successive exponential decays [46], similar to the one explained in Sec. 3.4. The existence of such a long-lived isomeric state with an associated $E2$ multipolarity of the $(7)^- \rightarrow (5)^-$ γ transition has not been discussed very elaborately in literature. The reader is referred to Sec. 4 for an interpretation based on the current work.

It is important to note that the 90-keV γ-ray of the $(9)^- \rightarrow (7)^-$ transition cannot be observed due to a large conversion coefficient, preventing the associated half-life to be determined. Therefore, the isomeric ratio of the $(9)^-$ state could not be evaluated. The half-life analysis regarding the $(7)^-$ state relied on the half-life value of the $(9)^-$ isomer extracted from a conversion electron measurement performed by Sun *et al* [50].

The isomeric ratios extracted from the present experiment are 18.5(10)% and 26.6(16)% for $I^\pi = (12)^+$ and $I^\pi = (7)^-$, respectively. The latter value is corrected for the feeding from the $I^\pi = (12)^+$ state.

4. Discussion

To interpret the improved and new results on isomeric states and isomeric ratios described in Sec. 3, shell-model calculations have been performed. They rely on the code NuShellX [51,52]. The calculations consider ^{208}Pb as the doubly-magic core and two interactions were probed:

- Poppelier and Glaudemans derived a particle-hole interaction around ^{208}Pb ($Z = 82$, $N = 126$) stretching in principle from $Z = 58$ to $Z = 114$ and from $N = 100$ to $N = 164$ [53]. In tables and figures, this interaction is labelled as 'pbpop' [51]. With ^{208}Pb as closed core, the Pb isotopes of interest are subject to a model space comprising neutron holes in the $1i_{13/2}$, $3p_{3/2}$, $2f_{5/2}$, and $3p_{1/2}$ orbitals. This is the present 'default' for the 'pbpop' interaction. For the heavier Pb isotopes the computational limits allow for probing two-particle two-hole, '2p-2h', excitations across the $Z = 82$ gap by allowing up to two holes in the $1h_{11/2}$ orbital and up to two particles in either of the $1h_{9/2}$ or $2f_{7/2}$ orbitals. To approach ^{198}Pb with the calculations, it is in any case necessary to retain at least ten neutrons in the high-j $1i_{13/2}$ orbital, 'pbpop-10'. One relevant constraint is that NuShellX is not yet optimized for large dimensions in either pure proton or pure neutron configurations, as in the case for Pb isotopes [54].
- The recommended [51] interaction for nuclei located 'South-West' from ^{208}Pb in the chart of nuclides is denoted 'khhe' [55]. It is adopted from an early Kuo-Herling interaction [56] and updated according to Ref. [57]. A more recent

adjustment of several two-body matrix elements (TBME) is proposed in Ref. [58] and applied to excited states in ^{204}Tl [59] and ^{204}Hg [60], respectively. Here we start with the 'default' interaction, covering all neutron orbitals between $N = 82$ and $N = 126$, namely $1h_{9/2}$, $2f_{7/2}$, $1i_{13/2}$, $3p_{3/2}$, $2f_{5/2}$, and $3p_{1/2}$. Calculations in the unrestricted neutron space are feasible for ^{206,204}Pb and for some low-lying states in ^{202}Pb. Thereafter, various truncation schemes were systematically tested to achieve the possibility to predict excited states in ^{198,200}Pb in a controlled manner [23]. Here, we refer to the subset:

- 'tr-9', which allows for at most one neutron hole each in the $1h_{9/2}$ and $2f_{7/2}$ orbitals;
- 'tr-f', which implies full occupation of the $1h_{9/2}$ and $2f_{7/2}$ orbitals and thus forms the same model space as 'pbpop-default';
- 'tr-f10', which in addition requires at least ten neutrons in the high-j $1i_{13/2}$ orbital (cf. 'pbpop-10');
- 'tr-f10M', for which the diagonal 0^+ two-body matrix-elements of the remaining $1i_{13/2}$, $3p_{3/2}$, $2f_{5/2}$, and $3p_{1/2}$ orbitals are systematically lowered according to $(N - 126) \cdot 50$ keV to handle missing contributions from pair fluctuations;
- 'tr-f10M' ', which stretches the predicted excitation schemes by a factor 1.1, thereby accounting for some over-binding of excited states.

The effects of these 'khhe' truncations and compensations will be detailed in the discussion of the ^{206,204}Pb predictions, displayed in Figs. 11 and 12.

Predicted $E2$ and $M1$ transition rates use standard effective charges, $e_{eff,p} = 1.5$ and $e_{eff,n} = 0.5$, and g factors of the free proton and neutron, respectively.

Finally, note that due to the quickly increasing dimensions the number of systematic large-scale shell-model surveys in the four quadrants around ^{208}Pb remains rather scarce [61, 62]. None of them tackles lighter Pb isotopes such as ^{198,200}Pb, for which particular numerical issues exist as large numbers of pure neutron configurations are concerned [54].

4.1. Decay Schemes

To establish a truncation scheme which allows shell-model calculations for ^{200}Pb and ^{198}Pb, a number of options were considered and tested on the well-known and computationally easy isotopes ^{206}Pb and ^{204}Pb. The relevant observed and predicted yrast sequences are shown in Figs. 11 and 12, respectively. Some $B(E2; 2^+ \rightarrow 0^+)$ values are presented and compared in Table 2.

As expected, both 'default' calculations reproduce the observed decay schemes very well, and in particular the (relative) position of the known isomeric states. In fact, one important message from the two figures is that the various truncations hardly affect the sequence of the yrast states. This implies that predicted spin-gap isomers persist. For instance, the 7^- in ^{206}Pb ($> 90\%$ ${i_{13/2}}^{-1} \otimes {p_{1/2}}^{-1}$) and the 9^- in ^{204}Pb ($\approx$ 60-70% ${i_{13/2}}^{-1} \otimes {f_{5/2}}^{-1}$), are present in any of the parametrizations. The 12^+ isomer in ^{206}Pb finds its explanation in the presence of a compressed high-j ${i_{13/2}}^{-2}$ multiplet, which leaves the alternatives of a low-energy $E2$ or slow $E3$ decay. In ^{204}Pb there is the observed 325-keV, $12^+ \rightarrow 11^-$ $E1$ alternative, in line with the predictions.

The 'tr-9' and 'tr-f;tr-f10' truncations on the 'khhe'-side lead to a compression of low-energy states, since more and more isoscalar 0^+ pair fluctuations are suppressed.

This can be reasonably well compensated for by increasing the attraction of the relevant TBME as defined above ('tr-f10M'), and subsequently stretching the whole decay scheme ('tr-f10M' '). For ^{204}Pb, the predictive power of the 'tr-f10M' ' truncation is essentially indistinguishable from the untruncated, 'khhe default', scheme. In case of ^{206}Pb, the position of the yrast 6^+ state is a significant difference between these two parametrizations, but this is simply due to the fact that 'khhe default' handles it as an almost pure (92%) ${h_{9/2}}^{-1} \otimes {f_{7/2}}^{-1}$ configuration. Closing those two orbitals (cf. 'pbpop'), however, implies that this option falls outside the configuration space.

Since the truncations hardly affect the effective number of partitions in ^{206}Pb, there is little to no effect observed on the calculated reduced transition rates. In fact, only by opening the $Z = 82$ shell (cf. 'pbpop 2p-2h') the predicted strengths approach the measured values for both ^{206}Pb and ^{204}Pb (see Table 2). Here one can note that the average occupation number of protons in the shells above $Z = 82$ is on the level of only 0.1. Hence, calculated excitation energies are only mildly modified, and improved if anything, when comparing the 'default' and '2p-2h' predictions for the 'pbpop' interaction.

Due to the current technical limitations indicated earlier [54], for ^{202}Pb only the 0^+, 2^+, and 4^+ sequence can be diagonalized for the 'khhe default' parametrization. Similarly, trying to calculate $B(E2; 2^+ \rightarrow 0^+)$ transition strengths fails for any of the 'pbpop' parameter sets, while it is possible to diagonalize very large dimensions (up to some 10^7) even for 'pbpop 2p-2h'.

The comparison between the isomer-related experimental yrast sequence and the predictions for ^{202}Pb is shown in Fig. 13. The 9^- spin-gap isomer (main configuration ${i_{13/2}}^{-1} \otimes f_{5/2}$) is reproduced by all calculations, in agreement with experiment. However, the energy gap between the yrast 7^- (${i_{13/2}}^{-1} \otimes {f_{5/2}}^{1}$) and 5^- (${i_{13/2}}^{-1} \otimes {p_{3/2}}^{-1}$) states is predicted somewhat smaller than observed, a pattern that persists toward the lighter Pb isotopes. Interestingly, on the 'pbpop' side, the inclusion of 2p-2h proton excitations improves the situation for ^{202}Pb. Additional correlations in primarily the low-spin states yield also an increased gap between the yrast 2^+ and 4^+ states, in agreement with experiment. The combined average occupation number of protons in the high-j shells above $Z = 82$ is on the level of only $0.10 - 0.15$.

Due to the existence and prediction of an 11^- level (${i_{13/2}}^{-1} \otimes (fp)^3$) below the 12^+ level (${i_{13/2}}^{-2}$), the latter is neither found nor predicted isomeric, similar to what happens in ^{204}Pb. The predicted compressed $14^+/16^+$ and $17^-/19^-$ multiplets readily explain the observed high-spin isomers in ^{202}Pb. Finally one can note that 'tr-f10M', provides a very good description, despite its artificial compression. Similarly, hardly any effect is seen when restricting the number of neutrons to at least ten in the $i_{13/2}$ orbital for 'pbpop-10', neither leads the inclusion of proton excitations to any significant improvement. The sequence of states and the position of the isomers is reproduced in any case.

Figure 14 provides the comparison between experiment and theory for ^{200}Pb. Technically, a 'khhe default' treatment is no longer possible. Therefore, the 'khhe' calculations are normalized to the 9^- isomer. In terms of nuclear structure, the situation in ^{200}Pb is very much alike the one in ^{202}Pb, with two differences: there is no 11^- level (predicted) below the 12^+ state, i.e. the latter is isomeric, in line with the observations. Secondly, while the 7^- and 9^- yrast states once more form a nearly degenerate multiplet, their sequence is changed in experiment and 'khhe' predictions. In turn, the somewhat more distant 5^- state is better reproduced with the 'pbpop' interaction and best reproduced for the calculation including 2p-2h proton excitations.

Similar to ^{200}Pb, the main improvements for the 'pbpop 2p-2h' scheme are increased energy gaps between the yrast 2^+ and 4^+ as well as 14^+ and 16^+ states, despite low average occupation numbers of ≈ 0.04 ($\pi(h_{9/2})$) and ≈ 0.09 ($\pi(f_{7/2})$). The $14^+/16^+$ and $17^-/19^-$ multiplets are described by both interactions, though somewhat better for 'khhe' compared with 'pbpop' parametrizations. The latter are too compressed, essentially due to the more schematic origin. Of course, this may be accounted for by adjusting selected TBME, but this is beyond the scope of this work, as the focus lies in the basic understanding of the medium-spin yrast sequence and the nature of the isomeric states. In this respect, the 'khhe tr-f10M' ' version is found to describe experiment very well.

The technical computational limits imply that calculations for ^{198}Pb in the pure neutron space are feasible only for a limited number of states for 'pbpop', and 'pbpop-10' as well as 'tr-f10M' '. At variance, it is possible to include 2p-2h proton excitations on top of the 'pbpop-10' space, thereby diagonalizing dimensions up to 10^7-10^8. The predictions are compared to the proposed experimental decay scheme of Ref. [48]. Note that starting with the 1823-keV state, the experimental spin values are tentative. From the point of view of excitation energies, the three predictions are in line with the observed level sequence, while the $2^+/4^+$, $5^-/7^-/9^-$, and $10^+/12^+$ multiplets are more compressed compared with experiment (see Fig. 15). For 'khhe tr-f10M' ' and 'pbpop 2p-2h', the predicted 12^+-9^- distance is considerably smaller than observed, a feature that has at least not been obvious for the heavier Pb isotopes.

Though being an extended calculation with very large dimensions, it is possible to predict transition rates between the low-spin yrast states even for the 'pbpop 2p-2h' parametrization. They are presented in Table 2. Similar to the experimentally known ^{204,206}Pb isotopes, there is an increase of a factor ≈ 3 when allowing for the proton excitations, despite merely identically small proton occupation numbers in the subshells above $Z = 82$ in ^{198}Pb compared with ^{200,202}Pb.

However, the major puzzle in this part of the ^{198}Pb decay scheme is the evaluated half-life of the $(7)^-$ level at 2141 keV: $T_{1/2} = 4.12(10)$ μs. With $E_\gamma = 318$ keV, this yields a tiny reduced transition strength of $B(E2) \approx 0.04$ e^{2}fm^4. At variance, both rather constrained calculations, which do not account for any proton excitations across $Z = 82$ either, call for $B(E2; 7^- \rightarrow 5^-)$ values of 1.1 ('pbpop-10') and 3.4 e^{2}fm^4 ('tr-f10M' '), respectively, i.e. almost two orders of magnitude larger. (Unfortunately, an attempt to derive transition rates for 'pbpop 2p-2h' failed for technical reasons [54].)

The inconsistency in predicted and observed 7^- half-life clearly deserves further, more detailed investigations, both theoretically and experimentally. In fact, already in Refs. [49, 50] the problem was noticed, and a solution suggested based on another 7^- state, supposedly decaying by a hitherto unobserved low-energy transition. Theoretically, such an additional level is likely to be present, though not yrare. While the latter is expected about 200 keV above the yrast 7^- state, a 6^-, 8^-, and 9^- multiplet is predicted within < 10 keV excitation energy, and just above the yrast 7^- state. Such a proximity of the even-spin negative parity 6^- and 8^- states to their odd-spin counterparts is neither observed nor predicted for any of the heavier Pb isotopes. This picture holds even for the 'pbpop 2p-2h' parametrization.

4.2. Isomeric Ratios

For isomeric states populated in fragmentation reactions, calculation of isomeric ratios is extremely difficult. The complex nature of the abrasion process, and the subsequent

deexcitation via nucleon emission makes it very hard to predict the spin distribution of the resultant evaporation residue. Even then, one must make some assumptions about how a particular isomer is fed by higher lying states. Abrasion-ablation model (ABRABLA) [64, 65] predictions for isomeric ratios are thus typically accurate only to within an order of magnitude [66]. As the model does not consider the properties of individual shell-model orbitals, only their average angular momenta, it is valid only for nuclei far from the projectile, typically $\Delta A > 10$.

In cases where only one or two nucleons are removed however, it is possible to predict isomeric ratios with some degree of accuracy. This relies on the fact that the residue of interest is populated predominantly via a direct reaction, and that there is no nucleon evaporation stage. One example is that of two-proton removal from ^{208}Pb, which, as discussed above, populates two isomeric states: 5^- and 10^+. This example was considered in detail in Refs. [20, 21]. In that case we can be sure that ^{206}Hg is populated by a direct, single-step mechanism due to the nucleon separation thresholds of the relevant isotopes. The indirect process — knockout of a single proton to ^{207}Tl to high excitation energy followed by evaporation of a second proton — is inhibited because $S_n(^{207}\mathrm{Tl}) < S_p(^{207}\mathrm{Tl})$ (7.368 MeV and 8.003 MeV respectively), and the fact that the proton is charged and its emission is therefore inhibited. This gives us confidence that when we observe ^{206}Hg it was created by a direct one-step process.

For the case of two neutron removal from ^{208}Pb producing ^{206}Pb, we have no such assurance. The neutron separation threshold for ^{207}Pb is lower than the proton threshold (6.738 MeV and 7.488 MeV respectively), and neutron emission is not inhibited by the Coulomb barrier. It is therefore possible that some fraction of the observed yield of ^{206}Pb is created via this indirect route. Predicting the associated cross section requires a reliable prediction of single particle spectroscopic factors up to high excitation energies in ^{207}Pb (6.7–15 MeV), and an understanding of how their neutron emission feeds into the states of ^{206}Pb, both of which are beyond the scope of the current discussion. The calculations presented here therefore assume a single-step direct reaction. We will, however, return to this discussion shortly.

The results presented here follow closely the analysis performed in Refs. [20, 21] for ^{208}Pb(-2p). The calculations assume eikonal reaction dynamics, such that the projectile and target follow a straight line trajectory [67, 68]. The core-target and nucleon-target interactions are calculated using a density folding approach, with densities taken from Skyrme Hartree-Fock calculations using the SkX interaction [69] (which reproduces the measured charge distribution of ^{208}Pb very well), and nucleon-nucleon cross sections using the parametrized form from Ref. [70]. The core is assumed to act as a spectator during its fast interaction with the target, such that states of the core are not coupled by this interaction.

The required two-nucleon amplitudes were taken from shell model calculations using the khhe [55] interaction. For this we used Oxbash [71] rather than NuShellX, due to technical problems in calculating the overlap amplitudes, though the results of the calculations are otherwise identical. The nucleon radial wave functions were calculated using a Woods-Saxon plus spin-orbit potential, the geometry parameters of which were constrained by the same Hatree-Fock calculations used to generate the densities used above. This gives a consistent description of the sizes of the core-target interaction and two-nucleon overlap function. Both two-nucleon stripping [67], and stripping-diffraction terms [68] were included, with the much smaller pure elastic breakup term being estimated.

The results for these calculations, along with those from Ref. [20] and the

macroscopic ABRABLA model [72] are shown in Table 3. It should be noted that the theoretical results from Ref. [20] include only known feeding, such that the theoretical value for the ^{206}Hg 5^- state is a lower limit. The present direct two-nucleon knockout calculations predict isomeric ratios of 11.2% and 2.3% for 7^- and 12^+ state, respectively, compared to the experimental values 23.7(16)% and 1.3(2)%, respectively. However, we expect there to be some contribution to the ^{206}Pb yield from indirect routes. How this changes the isomeric ratios depends on whether or not the states are fed by neutron evaporation, which in turn depends on their structure. The shell model calculations indicate that the 7^- state is predominantly a $\nu(i_{13/2}^{-1} \otimes p_{3/2})$ configuration, whereas the 12^+ state is pure $\nu i_{13/2}^{-2}$. Assuming that evaporation of low ℓ nucleons is preferred, we might expect there to be considerably more indirect feeding of the 7^- state (and states that γ-cascade into it) than the 12^+. The indirect route would then tend to enhance isomeric ratio of the 7^- relative to the 12^+, which is consistent with the deviation between the present calculations and experiment.

We may also consider how the isomeric ratio depends on the residue momentum. For direct two-nucleon knockout, the longitudinal momentum distribution is known to be strongly sensitive to the angular momentum coupling of the nucleon pair, which, when starting from a spin-0 projectile, translates into a sensitivity to the final state spin [73, 74]. The higher the spin, the wider the momentum distribution. As a result, the isomeric ratio for high-spin isomers may show a strong sensitivity to the residue momentum. This was seen, for example, for the 10^+ isomer in ^{206}Hg [21].

The experimental isomeric ratios as a function of momentum for ^{206}Pb and ^{198}Pb are shown in Fig. 16, and in both cases populate 7^- and 12^+ isomers. The residue momentum is derived from the spatial distribution of fragments in the same way as in Ref. [19]. For the ^{206}Pb cases, the 7^- isomeric ratio is flat, and nearly independent of the residue momentum. The 12^+ isomeric ratio is strongly peaked at the edges of the distribution. This is consistent with the 12^+ state being populated predominantly in a single direct process, that produces a wide momentum distribution, and hence peaking of the isomeric ratios at the extreme momenta. The 7^- state, if populated directly, should have a narrower momentum distribution than the 12^+, but may also be fed through neutron evaporation from ^{207}Pb. These facts lead to a nearly featureless isomeric ratio as a function of momentum.

The results for ^{206}Pb contrast with those for ^{198}Pb, where the isomeric ratios for the 7^- and 12^+ states are weakly dependent on the momentum. In ^{198}Pb, there is little difference between the 7^- and 12^+ cases, most likely due to their production via a more complex abrasion-ablation-type mechanism.

The isomeric states in nuclei further form the projectile (^{198,200,202}Pb) are populated mainly through two-step process, (multi-)neutron removal followed by neutron evaporation. For such cases the above described calculations are not feasible. Here we employed the ABRABLA model. The calculated isomeric ratios are shown in Table 3. One notes that the measured values for the high-spin $I^\pi = 19^-$ isomers in ^{200,202}Pb are much larger than the calculated ones. These isomers' dominant configuration is $\nu(i_{13/2}^{-3} \otimes f_{5/2}^{-1})$. Thus it includes three holes from the high-j $i_{13/2}$ orbital. The average j value of orbitals in this mass region is much lower. This might explain the large discrepancy between measured and predicted values for these high-spin isomers.

5. Summary

Isomeric states have been experimentally and theoretically studied in a series of Pb isotopes. A number of experimental observables have been improved, while by and large consistent with previous isomer studies of Pb isotopes of interest. A shell-model truncation scheme applicable toward ^{198,200}Pb has been developed and successfully tested along the isomer-dominated medium-spin yrast sequences of ^{198,200,202,204,206}Pb. Isomeric ratios have been systematically derived for ^{198,200,202,206}Pb and ^{206}Hg, the latter comparable with previous values. Comparisons with eikonal reaction model calculations show reasonable agreement for the isomeric ratios of ^{206}Pb, and though the 12^+ isomer should be populated directly, it's likely that the 7^- is partly produced via removal of a single neutron followed by neutron evaporation. This difference is evident in the dependence of the respective isomeric ratios on the ^{206}Pb momentum.

Given the relevance of the region and future research directions towards heavy, neutron-rich nuclei in the vicinity of ^{208}Pb, improved large-scale shell-model calculations with realistic interactions, liberated from present technical constraints, would be very valuable, leading to a more systematic and comprehensive understanding of the structure in this region.

Acknowledgments

The authors gratefully acknowledge the outstanding work of the GSI accelerator and ion-source crews in providing the experiment with the envisaged high beam intensities. Discussions with B.A. Brown and H. Grawe are highly appreciated and gratefully acknowledged. This work is supported by the European Community FP7-Capacities, contract ENSAR No. 262010 and by the Swedish Research Council (VR 2010-147 and VR 2013-4271). This work has also been supported by the BMBF under Grant Nos. 05P09RDFN4, 05P12RDFN8, 05P15RDFN1, 05P11PKFNE, and 05P15PKFNA, by the LOEWE center HIC for FAIR, by the Science and Technology Facilities Council, and by Australian Research Council Grant Nos. FT120100760 and DP170102423. A. Gadea activity has been partially supported by MINECO and Generalitat Valenciana, Spain, grants FPA2014-57196-C5, Severo Ochoa and PROMETEO II/2014/019 and by the E.C. FEDER funds.

References

[1] Walker P and Dracoulis G 1999 *Nature* (London) **399** 35
[2] Grzywacz R *et al* 1995 *Phys. Lett.* B **355** 439
[3] M. Pfützner *et al* 1998 *Phys. Lett.* B **444** 32
[4] Podolyák Zs *et al* 2000 *Phys. Lett.* B **491** 225
[5] Geissel H *et al* 1992 *Nucl. Instrum. Methods* B **70** 286
[6] Pietri S *et al* 2007 *Nucl. Instrum. Methods* B **261** 1079
[7] Regan P H *et al* 2007 *Nucl. Phys.* A **787** 491c
[8] Rudolph D *et al* 2008 *Phys. Rev.* C **78** 021301(R)
[9] Nara Singh B S *et al* 2011 *Phys. Rev. Lett.* **107** 172502
[10] Jungclaus A *et al* 2007 *Phys. Rev. Lett.* **99** 132501
[11] Steer S J *et al* 2008 *Phys. Rev.* C **78** 061302(R)
[12] Gottardo A *et al* 2013 *Phys. Lett.* B **725** 292
[13] Söderström P-A *et al* 2013 *Nucl. Instrum. Methods* B **317** 649
[14] Watanabe H 2016 *EPJ Web of Conferences* **123** 02007
[15] Podolyák Zs *et al* 2009 *Phys. Lett.* B **672** 116

[16] Denis Bacelar *et al* 2013 *Phys. Lett.* B **723** 302
[17] Schmidt-Ott W-D *et al* 1994 *Z. Phys.* A **350**, 215
[18] Kmiecik M *et al* 2010 *Eur. Phys. J.* A **45** 153
[19] Podolyák Zs *et al* 2016 *Phys. Rev. Lett.* **117** 222302
[20] Simpson E C, Tostevin J A, Podolyák Zs, Regan P H and Steer S J 2009 *Phys. Rev.* C **80** 064608
[21] Simpson E C, Tostevin J A, Podolyák Zs, Regan P H and Steer S J 2010 *Phys. Rev.* C **82** 037602
[22] Pietralla N *et al* 2014 *EPJ Web of Conferences* **66** 02083
[23] Lalović N 2017 *PhD thesis* Lund University ISBN 978-91-7753-288-0 via portal.research.lu.se/portal/en
[24] Alexander T *et al* 2015 *Acta Phys. Pol.* **46** 601
[25] Alexander T 2015 *PhD thesis* University of Surrey
[26] Pfützner M *et al* 2002 *Phys. Rev.* C **65** 064604
[27] Stolz A *et al* 2002 *Phys. Rev.* C **65** 064603
[28] Akkoyun S *et al* 2012 *Nucl. Instrum. Methods* **A668** 26
[29] Ralet D *et al* 2017 *Phys. Rev.* C **95** 034320
[30] Ralet D *et al* 2015 *Nucl. Instrum. Methods* **A786** 32
[31] Lalović N *et al* 2016 *Nucl. Instrum. Methods* **A806** 258
[32] Golubev P *et al* 2013 *Nucl. Instrum. Methods* **A723** 55
[33] Lalović N *et al* 2015 *EPJ Web of Conferences* **93** 07007
[34] Venturelli R and Bazzacco D 2004 *LNL Annual Report* **2004** 220
[35] Kibèdi T, Burrows T W, Trzhaskovskaya M B, Davidson P M and Nestor Jr C W, 2008 *Nucl. Instrum. Methods* **A589** 202
[36] Podolyák Zs. *et al* 2003 *Nucl. Phys. A* **722** C273
[37] Kondev F G 2008 *Nuclear Data Sheets* **109** 1527
[38] Fornal B *et al* 2001 *Phys. Rev. Lett.* **87** 212501
[39] Steer S J *et al* 2011 *Phys. Rev.* C **84** 044313
[40] Draper J E, McDonald R J and King N S P 1977 *Phys. Rev.* C **16** 1594
[41] Stenzel Ch, Grawe H, Haas H, Mahnke H-E and Maier K H 1983 *Nucl. Phys.* A **411** 248
[42] Poletti A R, Dracoulis G D, Byrne A P, Stuchberry A E, Fabricius B, Kibèdi T and Davidson P M 1994 *Nucl. Phys.* A **580** 43
[43] Zhu S and Kondev F G 2008 *Nuclear Data Sheets* **109** 699
[44] Fant B, Weckström T, Jain H C, Norlin L O, Rensfelt K-G, Carle P and Rosengård U 1987 *Nucl. Phys.* A **475** 338
[45] Rudolph D *et al* 2008 *Eur. Phys. J.* A **36** 131
[46] Bateman H 1910 *Proc Cambridge Philos Soc* **15** 423
[47] Kondev F G and Lalkovski S 2007 *Nuclear Data Sheets* **108** 1471
[48] Xiaolong H and Mengxiao K 2016 *Nuclear Data Sheets* **133** 221
[49] Stenzel C, Grawe H, Haas H, Mahnke H-E and Maier K H 1985 *Z. Phys.* A **322** 83
[50] Sun X, Rosengård U, Grawe H, Haas H, Kluge H, Kuhnert A, and Maier K H 1989 *Z. Phys.* A **333** 281
[51] Brown B A and Rae W D M 2014 *Nuclear Data Sheets* **120** 115
[52] Brown B A 2001 *Prog. Part. Nucl. Phys.* **47** 517
[53] Poppelier N A F M and Glaudemans P W M 1988 *Z. Phys.* A **329** 275
[54] Brown B A priv. comm.
[55] Warburton E K and Brown B A 1991 *Phys. Rev.* C **43** 602
[56] McGrory J B and Kuo T T S 1975 *Nucl. Phys.* A **247** 283
[57] Rydström L, Blomqvist J, Liotta R J and Pomar C 1990 *Nucl. Phys.* A **512** 217
[58] Szpak B *et al* 2011 *Phys. Rev.* C **83** 064315
[59] Broda R *et al* 2011 *Phys. Rev.* C **84** 014330
[60] Wrzesiński J *et al* 2015 *Phys. Rev.* C **92** 044327
[61] Caurier E, Rejmund M and Grawe H 2003 *Phys. Rev.* C **67** 054310
[62] Teruya E, Higashiyama K and Yoshinaga N 2016 *Phys. Rev.* C **93** 064327
[63] Chiara C J and Kondev F G 2010 *Nuclear Data Sheets* **111** 141
[64] Gaimard J-J and Schmidt K-H 1991 *Nucl. Phys.* A **531** 709
[65] de Jong M, Ignatyuk A and Schmidt K-H 1997 *Nucl. Phys.* A **613** 435
[66] Bowry M *et al* 2013 *Phys. Rev.* C**88** 024611
[67] Tostevin J A *et al* 2004 *Phys. Rev.* C **70** 064602
[68] Tostevin J A and Brown B A 2006 *Phys. Rev.* C **74** 047302
[69] B. A. Brown 1998 *Phys. Rev.* C **58** 220

[70] Ray L 1979 *Phys. Rev.* C **20** 1857
[71] Brown B A *et al* MSU-NSCL report number 1289
[72] Ricciardi M V priv. comm.
[73] Simpson E C *et al* 2009 *Phys. Rev. Lett.* **102** 132502
[74] Simpson E C *et al* 2009 *Phys. Rev.* C **79** 064621

Figure captions

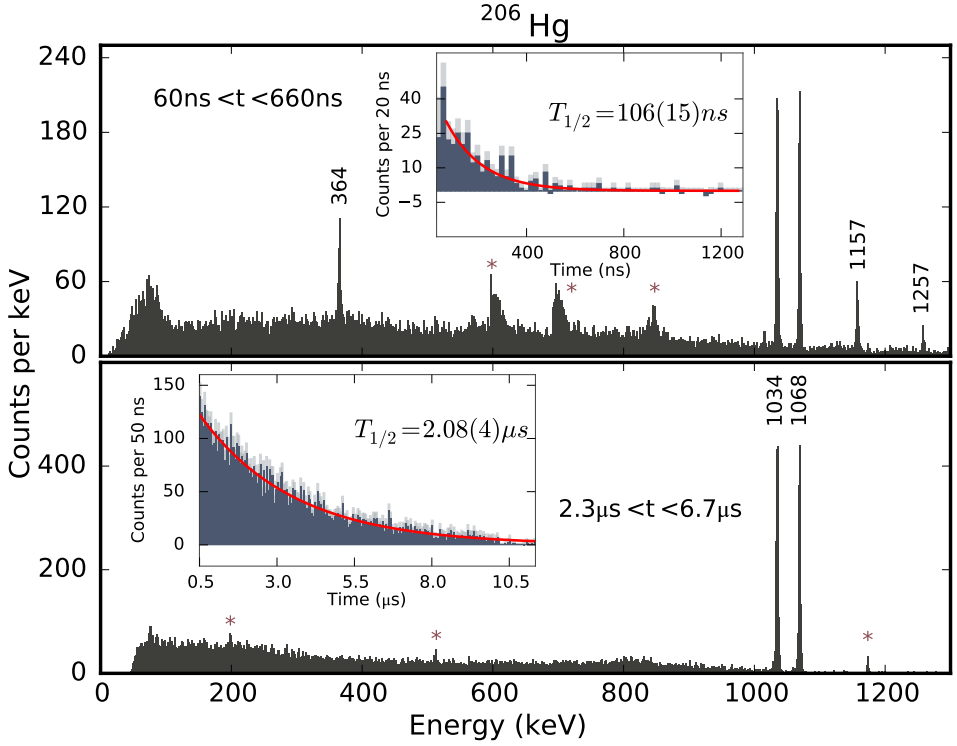

Figure 1. Delayed γ-ray spectra recorded after the implantation of ^{206}Hg ions. The peaks labelled with their energies in keV represent the transitions used to measure half-lives, whereas known background contributions are indicated by stars (*). The two panels show relevant transitions following the decay of the $I^{\pi} = 10^{+}$ isomeric state (upper panel) and those originating from the $I^{\pi} = 5^{-}$ state (lower panel). The two spectra are obtained for different time ranges: (*top*) 60 ns $< t <$ 660 ns; (*bottom*) 2.3 μs $< t <$ 6.7 μs. The insets show the decay curves of the two isomers: (*top*) as a result of the transitions at 1157 and 1257 keV; (*bottom*) as a result of the transitions at 1034 and 1068 keV. The experimental data are plotted as solid histograms and the light grey areas mark the experimental uncertainties. The solid line (red) is obtained from the least-squares fitting procedure of the exponential decay.

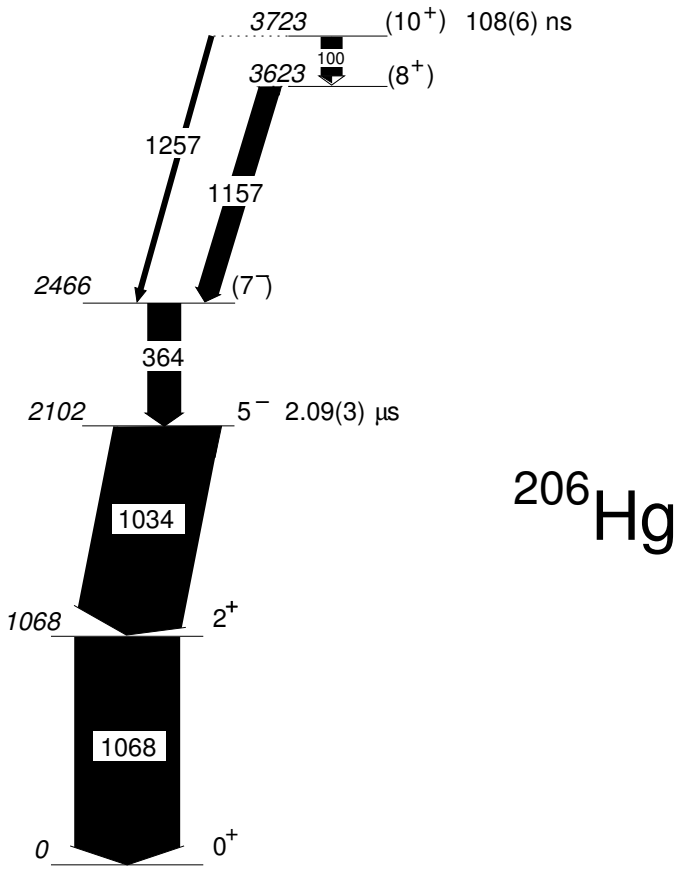

Figure 2. Partial decay scheme of two isomeric states in ^{206}Hg measured in the present work. Half-life values are the adopted values from this analysis and previous experiments. The widths of the arrows correspond to the relative intensities observed in the present isomer study (cf. Table 1).

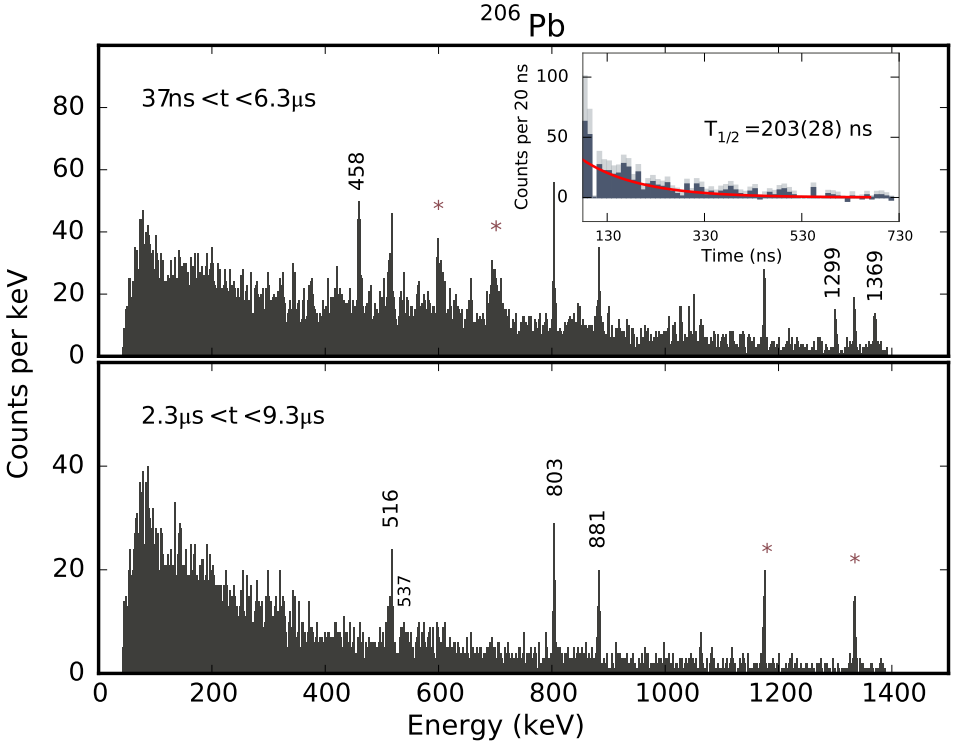

Figure 3. Delayed γ-ray spectra recorded after the implantation of ^{206}Pb ions. The two panels show relevant transitions following the decay of the $I^{\pi} = 12^{+}$ isomeric state (upper panel) and those originating from the $I^{\pi} = 7^{-}$ state (lower panel). The two spectra are obtained for different time ranges: (*top*) 37 ns $< t <$ 6.3 μs; (*bottom*) 2.3 μs $< t <$ 9.3 μs. The transitions relevant for the present analysis are labelled with energies in keV, whereas the known background contributions are indicated by stars (*). The inset shows the decay curve of the $I^{\pi} = 12^{+}$ isomer as a result of the transitions at 458, 1299, and 1369 keV; The experimental data are plotted as solid histograms and the light grey area marks the experimental uncertainties. The solid line (red) is obtained from the least-squares fitting procedure of the exponential decay.

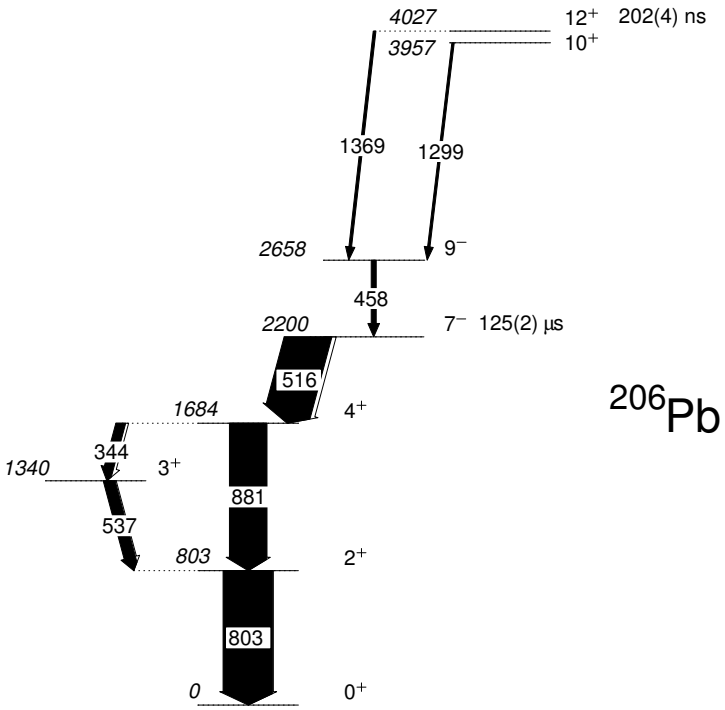

Figure 4. Partial decay scheme of two isomeric states in ^{206}Pb measured in the present work. Half-life values are the adopted values from this analysis and previous experiments. The widths of the arrows correspond to the relative yield observed in the present isomer study (cf. Table 1).

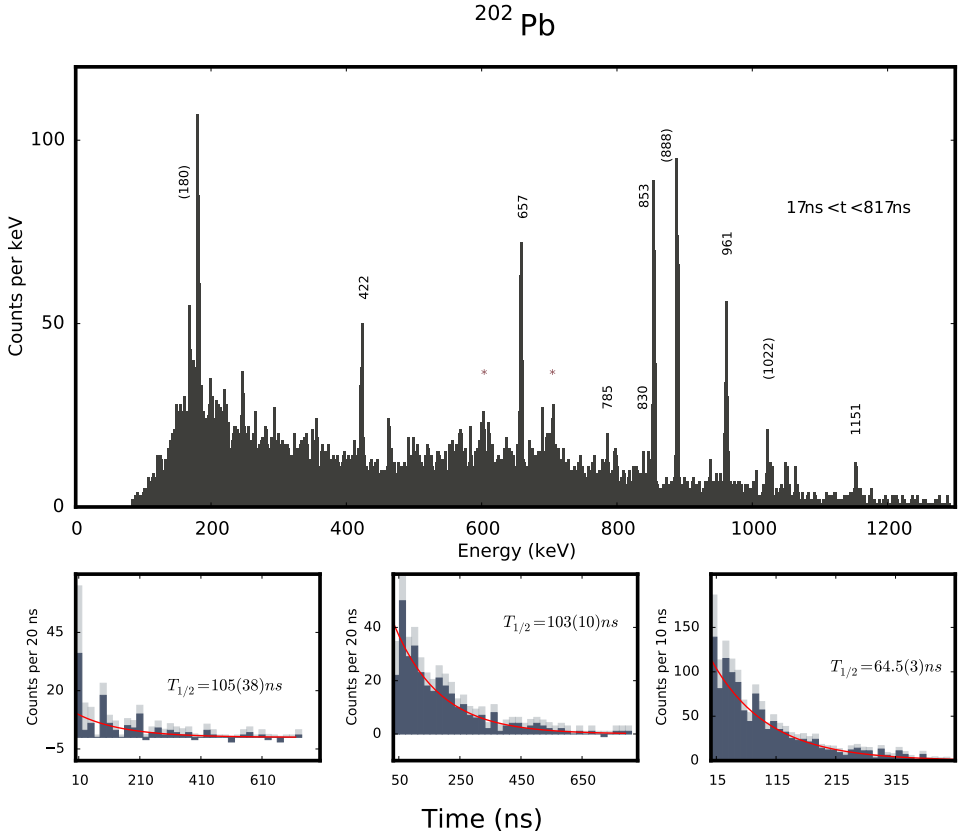

Figure 5. Delayed γ-ray spectrum recorded after the implantation of ^{202}Pb ions (upper panel). The spectrum is obtained for the time range 17 ns $< t <$ 817 ns. The transitions following the decays of the $I^{\pi} = 19^{-}$, and relevant for the present analysis are labelled with energies in keV, whereas the energies in brackets indicate the transitions not used in the isomeric ratio analysis. The known background contributions are indicated by stars (*). The decay curves of the isomers are shown in the lower panel: (*left*) $I^{\pi} = 19^{-}$ as a result of the transitions at 1151 and 797 keV; (*middle*) $I^{\pi} = 16^{+}$ as a result of the transition at 853 keV; (*right*) $I^{\pi} = 7^{-}$ as a result of the transitions at 657, 422, and 961 keV. Note that the transition at 888 keV was not considered for the half-life determination of $I^{\pi} = 16^{+}$, due to the presence of the $I^{\pi} = 12^{+}$ isomeric state (see Fig. 6) with the reported half-life of 24.4(3) ns [43]. The experimental data are plotted as solid histograms and the light grey areas mark the experimental uncertainties. The solid lines (red) are obtained from the least-squares fitting procedure of the exponential decay.

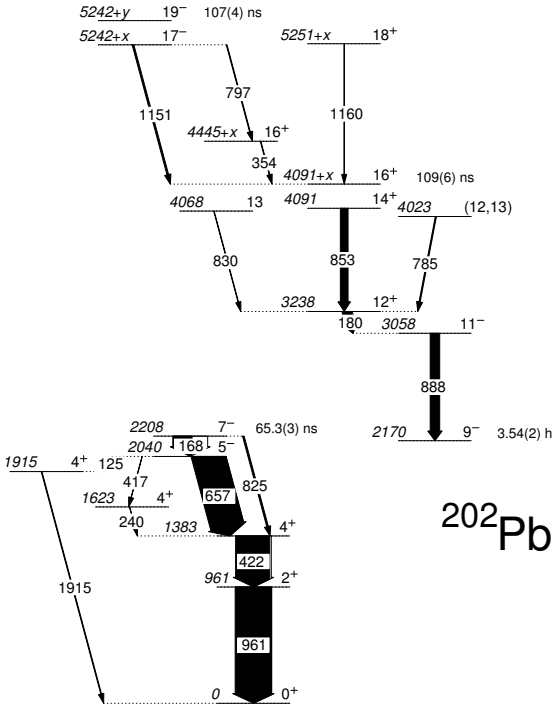

Figure 6. Partial decay scheme of three isomeric states in ^{202}Pb measured in the present work. Half-life values are the adopted values from this analysis and previous experiments. The widths of the arrows correspond to the relative yield obsered in the present isomer study (cf. Table 1).

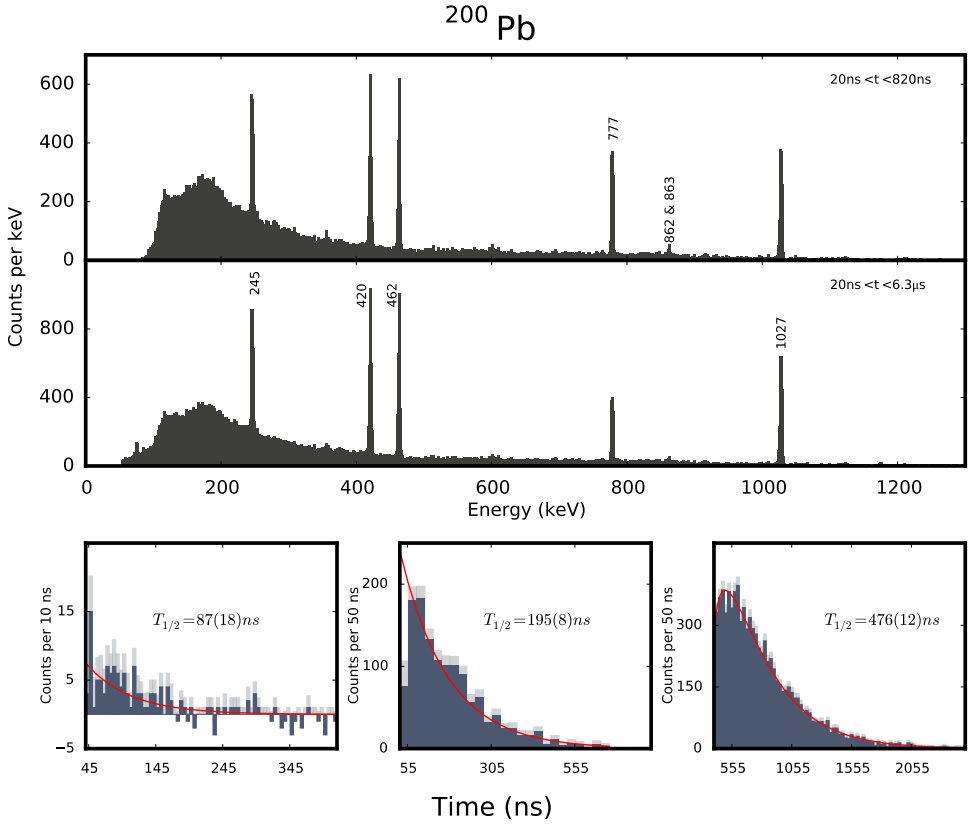

Figure 7. Delayed γ-ray spectra recorded after the implantation of ^{200}Pb ions. The two upper panels show relevant transitions following the decays of the $I^\pi = (19^-)$ isomeric state, $I^\pi = (12^+)$ and those originating from the $I^\pi = (9^-)$ state. The spectra are obtained for different time ranges, 20 ns $< t <$ 820 ns and 20 ns $< t <$ 6.3 μs. The transitions relevant for the present analysis are labelled with energies in keV. The decay curves of the isomers are plotted in the lower panel: (*left*) $I^\pi = (19^-)$ as a result of the 862/863-keV doublet; (*middle*) $I^\pi = (12^+)$ as a result of the transition at 777 keV; (*right*) $I^\pi = (9^-)$ as a result of the transitions at 420, 462, and 1027 keV. Note that the half-life analysis of $I^\pi = 12^+$ showed that the effect of feeding from $I^\pi = 19^-$ isomer is negligible. The experimental data are plotted as solid histograms and the light grey areas mark the experimental uncertainties. The solid lines (red) are obtained from the least-squares fitting procedure of the exponential decay.

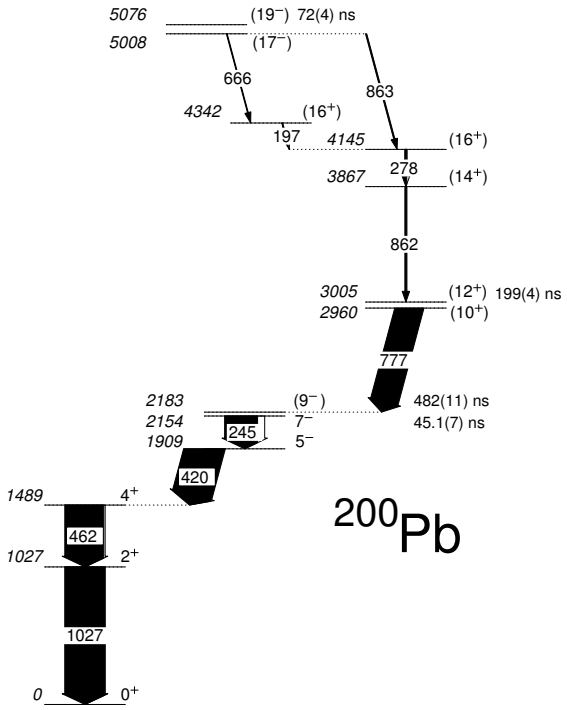

Figure 8. Partial decay scheme of isomeric states in ^{200}Pb measured in the present work. Half-life values are the adopted values from this analysis and previous experiments, with the exception of the $I^{\pi} = 7^{-}$ half-life, which is the one available in the literature [47]. The widths of the arrows correspond to the relative yield observed in the present isomer study (cf. Table 1).

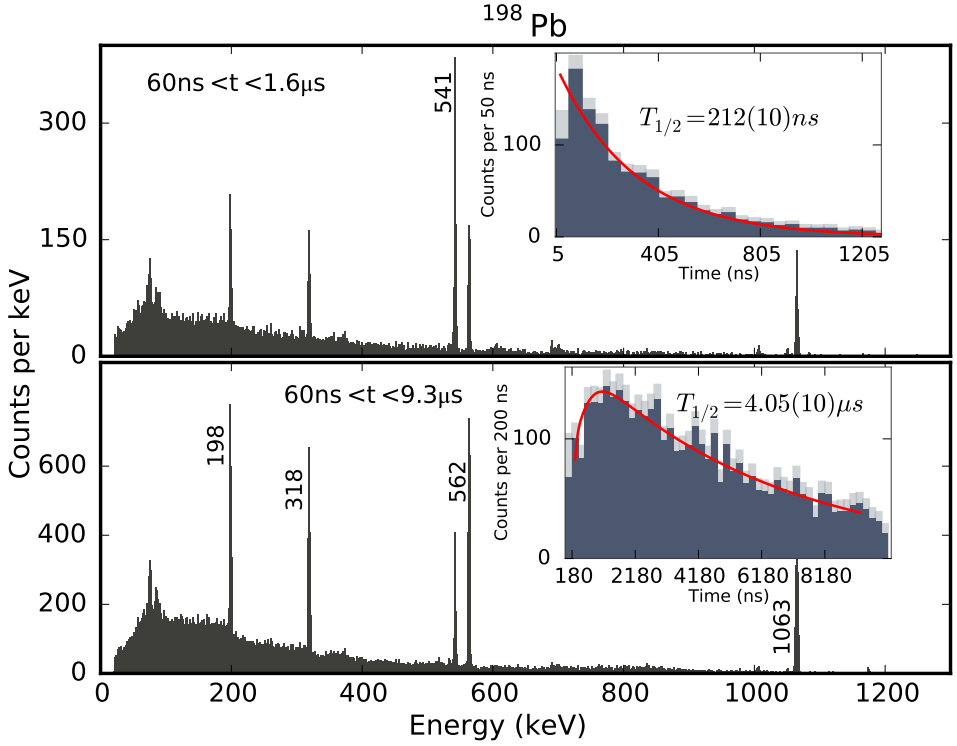

Figure 9. Delayed γ-ray spectra recorded after the implantation of ^{198}Pb ions. The two panels show relevant transitions following the decay of the $I^{\pi} = (12)^{+}$ isomeric state (upper panel) and those originating in the $I^{\pi} = (7)^{-}$ state (lower panel). The two spectra are obtained for different time ranges: (*top*) 60 ns $< t <$ 1.6 μs; (*bottom*) 60 ns $< t <$ 9.3 μs. The transitions relevant for the present analysis are labelled with energies in keV. The inset shows the decay curves of the two isomers: (*top*) as a result of the transition at 541 keV; (*bottom*) as a result of the transitions at 562 and 1063 keV. The experimental data are plotted as solid histograms and the light grey area marks the experimental uncertainties. The solid line (red) is obtained from the least-squares fitting procedure of the exponential decay.

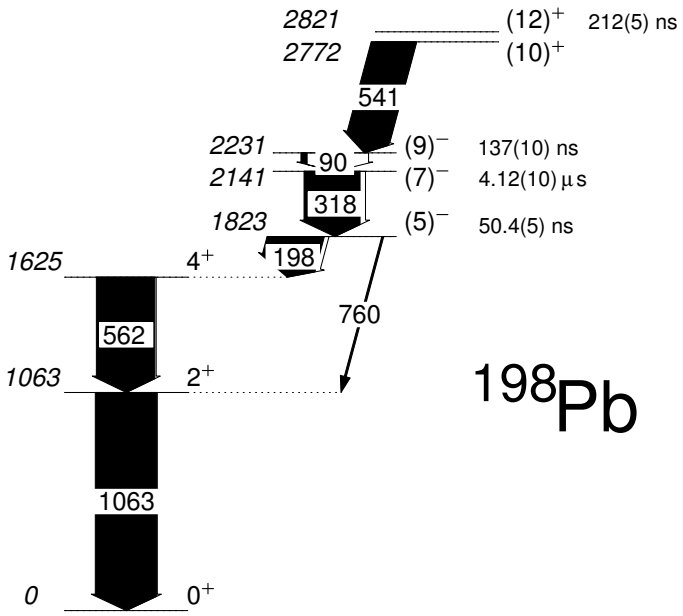

Figure 10. Partial decay scheme of isomeric states in ^{198}Pb measured in the present work. Half-life values of $I^{\pi} = (12)^{+}$ and $I^{\pi} = (7)^{-}$ are the adopted values from this analysis and previous experiments, whereas the ones regarding the levels $I^{\pi} = (9)^{-}$ and $I^{\pi} = (5)^{-}$ are literature values [48]. The widths of the arrows correspond to the relative yield observed in the present isomer study (cf. Table 1).

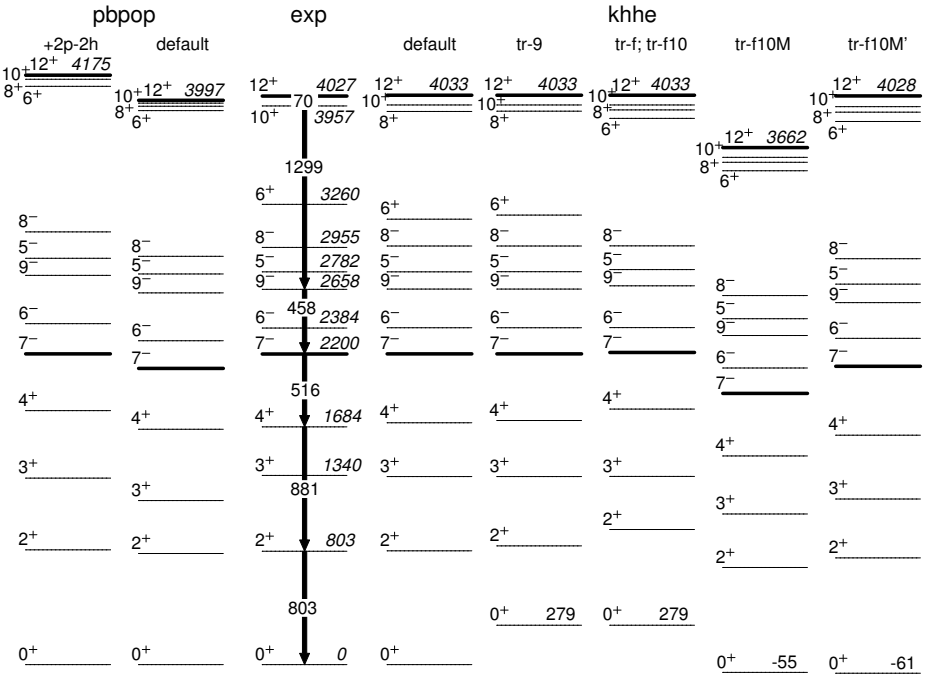

Figure 11. Comparison between experimental ('exp') [37] and predicted ('pbpop', 'khhe') decay schemes of ^{206}Pb starting from the 12^+ isomer. Isomeric states are indicated by thick horizontal lines. All states are labelled with spin and parity, selected ones also with their excitation energy in keV. The main experimental γ-ray cascade is included for reference. Both 'pbpop' and the 'khhe default' calculations are normalized to the 0^+ ground state, the other 'khhe' schemes are presented relative to the 'default' ground state.

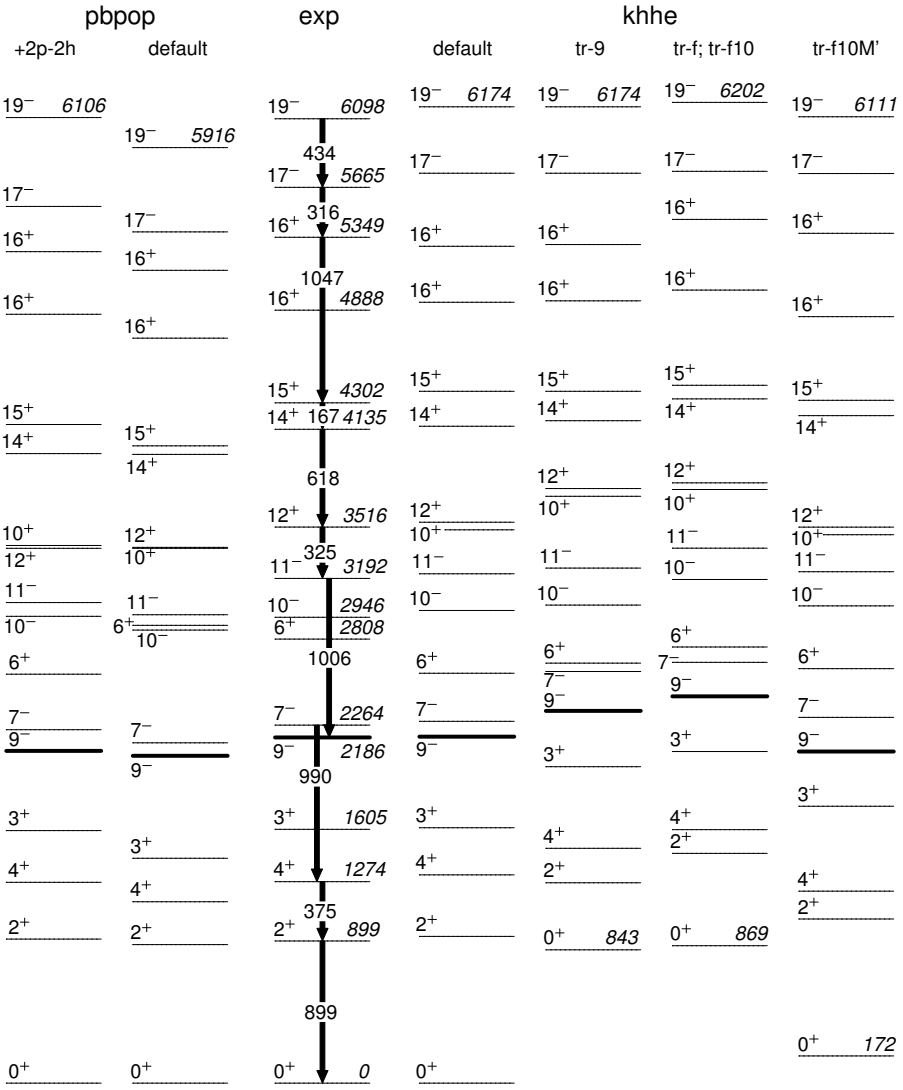

Figure 12. Comparison between experimental ('exp') [63] and predicted ('pbpop', 'khhe') decay schemes of ^{204}Pb starting from the 19^- isomer. Isomeric states are indicated by thick horizontal lines. All states are labelled with spin and parity, selected ones also with their excitation energy in keV. The main experimental γ-ray cascade is included for reference. Both 'pbpop' and the 'khhe default' calculations are normalized to the 0^+ ground state, the other 'khhe' schemes are presented relative to the 'default' ground state.

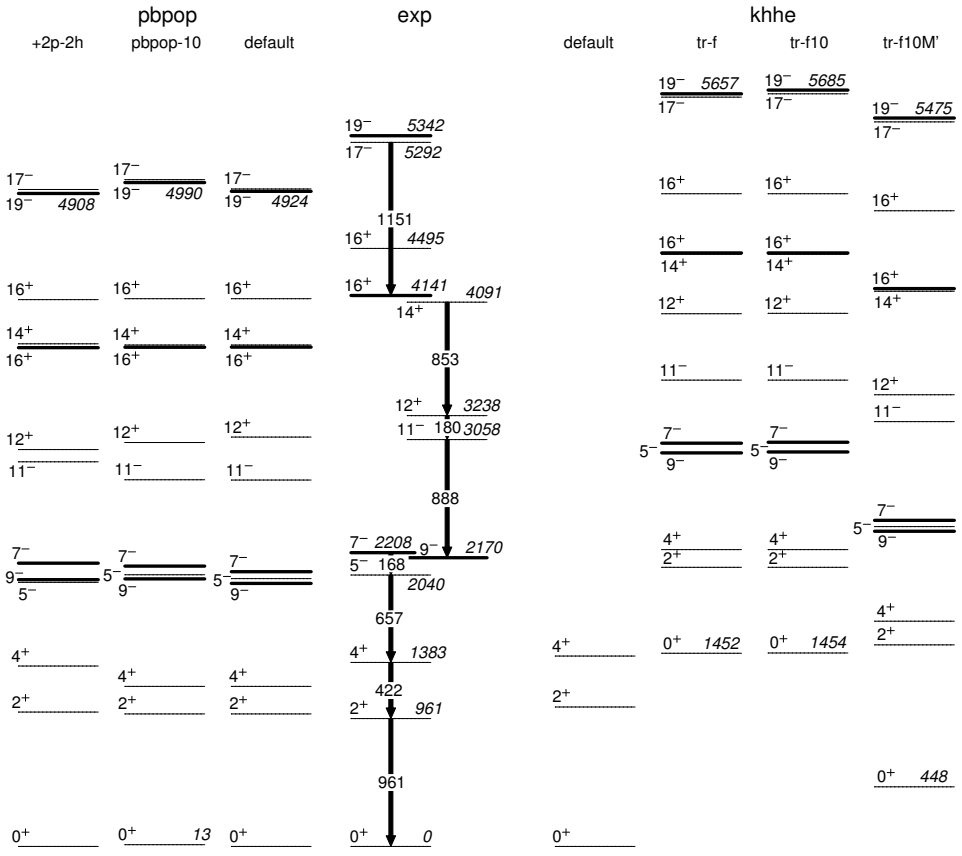

Figure 13. Comparison between experimental ('exp') [43] and predicted ('pbpop', 'khhe') decay schemes of ^{202}Pb starting from the 19^- isomer. Isomeric states are indicated by thick horizontal lines. All states are labelled with spin and parity, selected ones also with their excitation energy in keV. The main experimental γ-ray cascade is included for reference. The two 'default' calculations are normalized to the 0^+ ground state, the other schemes are presented relative to their respective 'default' ground state. The 'khhe default' calculation was technically not feasible for the states above $I^\pi = 4^+$.

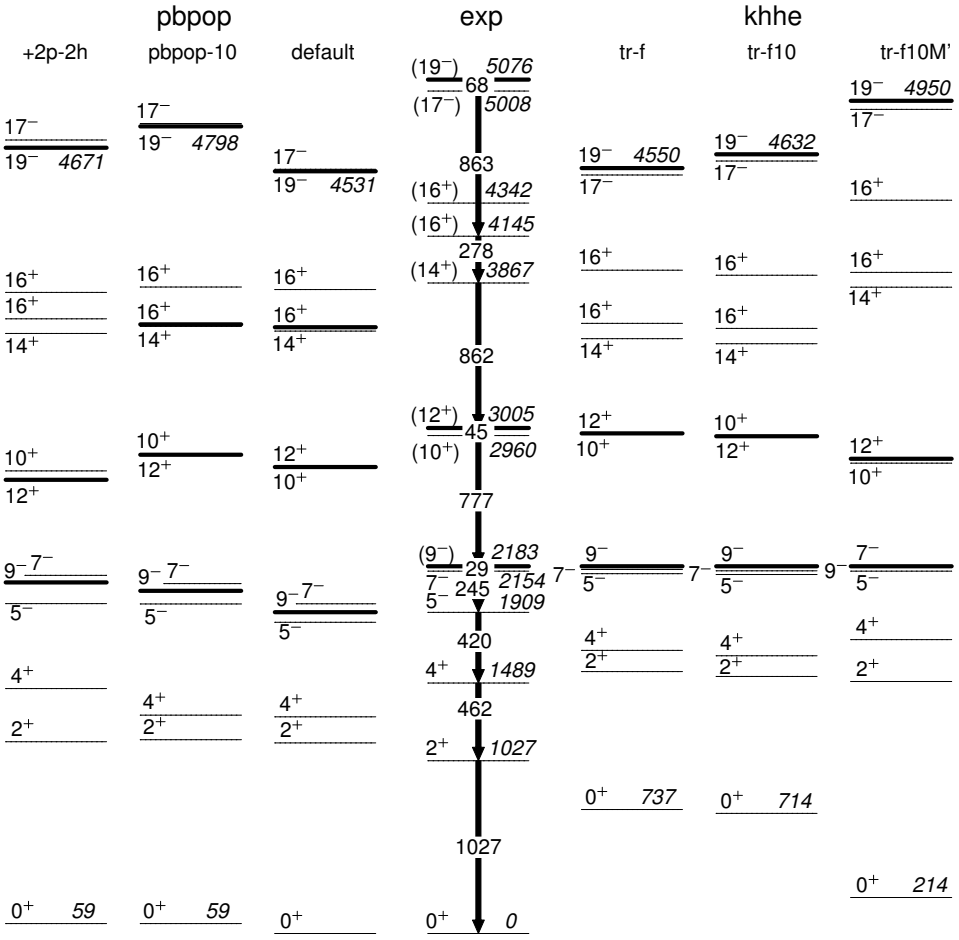

Figure 14. Comparison between experimental ('exp') [47] and predicted ('pbpop', 'khhe') decay schemes of ^{200}Pb starting from the 19^- isomer. Isomeric states are indicated by thick horizontal lines. All states are labelled with spin and parity, selected ones also with their excitation energy in keV. The main experimental γ-ray cascade is included for reference. The 'pbpop default' calculation is normalized to the 0^+ ground state, 'pbpop-10' is presented relative to that, and the '+2p-2h' prediction aligned to the latter. All 'khhe' decay schemes are normalized to the experimental 9^- isomer.

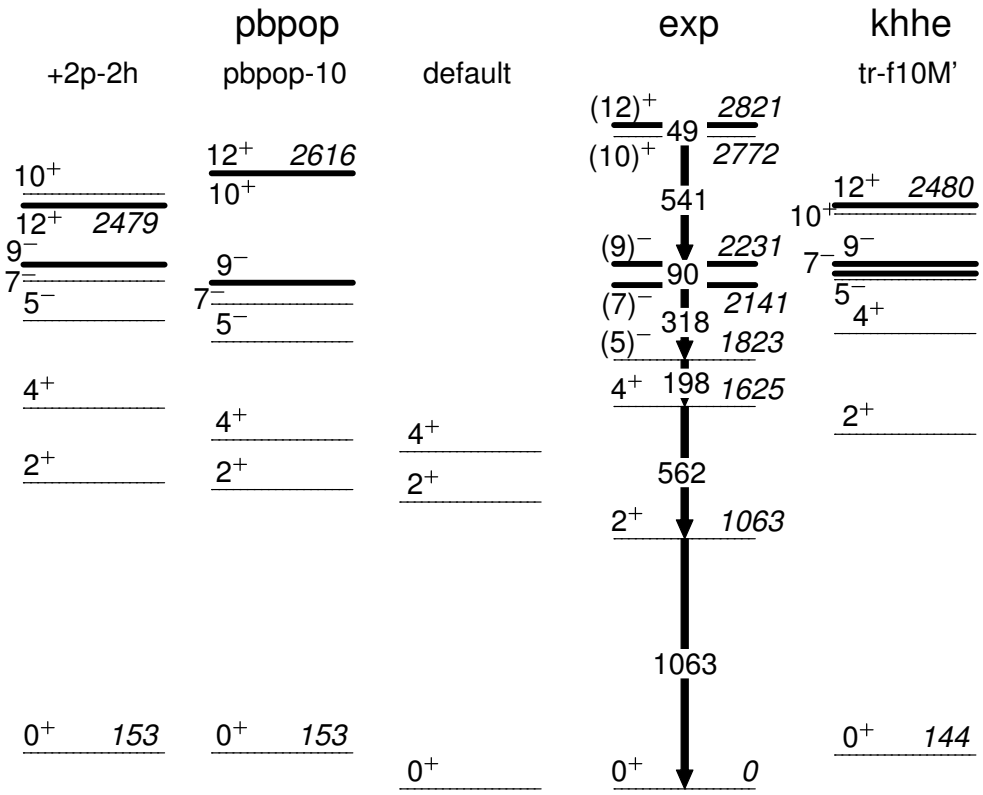

Figure 15. Comparison between experimental ('exp') [48] and predicted ('pbpop', 'khhe') decay schemes of ^{198}Pb starting from the $(12)^+$ isomer. Isomeric states are indicated by thick horizontal lines. All states are labelled with spin and parity, selected ones also with their excitation energy in keV. The main experimental γ-ray cascade is included for reference. The 'pbpop default' calculation is normalized to the 0^+ ground state, 'pbpop-10' is presented relative to that, and the '+2p-2h' prediction aligned to the latter. The 'khhe tr-f10M" decay scheme is normalized to the experimental $(9)^-$ isomer.

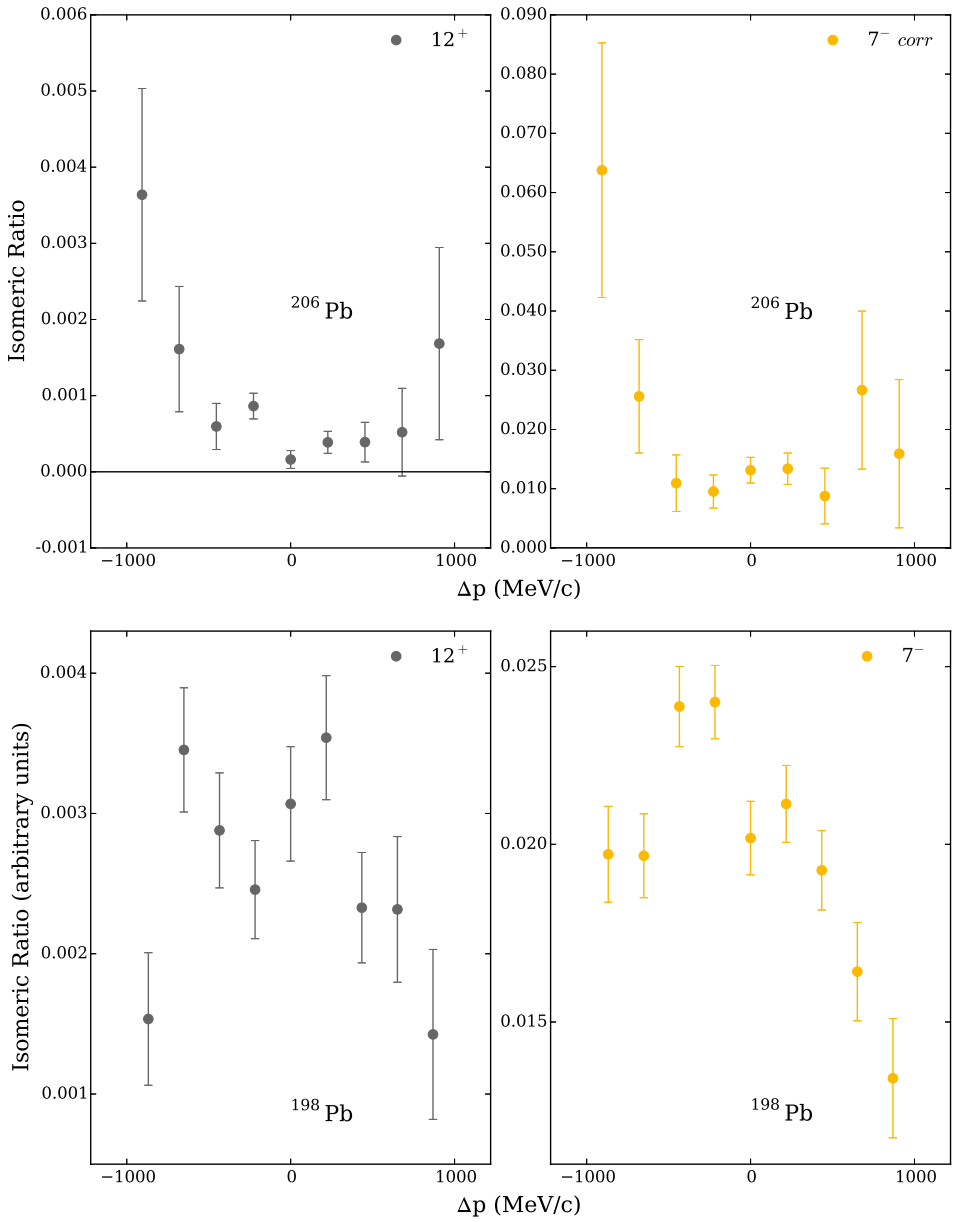

Figure 16. Isomeric ratios of the 12^+ (left column) and 7^- (right column) isomeric states in ^{206}Pb (top row) and ^{198}Pb (bottom row) as function of the longitudinal momentum of the ions measured at the intermediate focal plane of the fragment separator. Note that the momentum distribution for the 7^- state in ^{206}Pb is obtained by excluding the feeding from the 12^+ state. Horizontal lines denote the value of zero isomeric ratio.

Tables and table captions

Table 1. Summary of quantities relevant for the observed isomeric states. Isotope, spin and parity, I^π, half-live values, $T_{1/2}$, from the present analysis and adopted, associated γ rays, E_γ, and isomeric ratios, R_{exp}, are listed. For the corresponding decay schemes, see Figs. 2, 4, 6, 8, and 10.

	I^π ($\hbar$)	$T_{1/2}$ present	$T_{1/2}$ adopted	E_γ (keV)	R_{exp} (%)
^{206}Hg	10^+	106(15) ns	108(6) ns	1257	4.4(6)
				1157	3.2(3)
				364	3.5(4)
				weighted average:	3.5(2)
	5^-	2.08(4) μs	2.09(3) μs	1034	34.2(18)
				1068	32.4(18)
				weighted average:	29.7(13)[a]
^{206}Pb	12^+	203(28) ns	202(4) ns	1369	1.3(3)
				1299	1.2(3)
				458	1.5(3)
				weighted average:	1.3(2)
	7^-		125(2) μs	516	21.0(27)
				881	26.4(32)
				537	21.9(71)
				803	24.9(27)
				weighted average:	22.4(16)[b]
^{202}Pb	19^-	105(38) ns	107(4) ns	1160	0.6(4)
				797	1.0(4)
				1151	0.5(1)
				weighted average:	0.5(1)
	16^+	103(10) ns	109(6) ns	853	2.6(3)
				830	3.6(20)
				785	2.6(9)
				weighted average:	2.2(3)[C]
	7^-	64.5(3) ns	65.3(3) ns	657	9.5(13)
				422	8.3(11)
				961	9.3(12)
				weighted average:	9.0(7)
^{200}Pb	(19^-)	87(18) ns	72(4) ns	666	0.6(5)
				862[d]	0.8(2)
				weighted average:	0.8(2)
	(12^+)	195(8) ns	199(4) ns	777	14.2(7)
				weighted average:	13.4(8)[c]

	I^π ($\hbar$)	$T_{1/2}$ present	$T_{1/2}$ adopted	E_γ (keV)	R_{exp} (%)
^{200}Pb	(9^-)	476(12) ns	482(11) ns	245	35.7(16)
				420	33.9(15)
				462	32.0(14)
				1027	31.0(14)
				weighted average:	19.5(10)[b]
	$(12)^+$	212(10) ns	212(5) ns	541	18.5(10)
^{198}Pb	(7^-)	4.05(10) μs	4.12(10) μs	318	45.4(21)
				562	44.9(21)
				1063	45.0(20)
				weighted average:	26.6(16)[b]

[a] Corrected for feeding from the $I^\pi = 10^+$ state.
[b] Corrected for feeding from the $I^\pi = 12^+$ state.
[c] Corrected for feeding from the $I^\pi = 19^-$ state.
[d] Corresponds to 862/863-keV doublet [47].

Table 2. Experimental (exp) and calculated (khhe; pbpop) reduced transition strengths, $B(E2; 2^+ \to 0^+)$ (e^{2}fm^4), for ^{206}Pb, ^{204}Pb, and ^{198}Pb.

	exp	khhe				pbpop	
	[37, 63]	default	tr-9	tr-f10	tr-f10M	default	+2p-2h
^{206}Pb	204(6)	57	55	50	50	65	168
^{204}Pb	335(4)	91	61	50	55	84	222
^{198}Pb	n/a	–	–	–	86	71	226[a]

[a] The minimum number of neutrons in the $i_{13/2}$ subshell is set to 10.

Table 3. Summary of experimental (R_{exp}) and theoretical (R_{th} and $R_{th}^{ABRABLA}$) isomeric ratios determined in the current work. Note that theoretical predictions do not consider feeding corrections. Therefore, the experimental values quoted here are not corrected for the observed feeding either. See text for details.

Nucleus	Isomer I_i^π	R_{exp} (%) current work	R_{exp} (%) previous works	R_{th} (%)	$R_{th}^{ABRABLA}$ (%)
^{206}Hg	10^+	3.5(2)	2.2(7) [39]	4.7	
	5^-	33	21.9(15) [39]	18.8	
^{206}Pb	12^+	1.3(2)		2.3	
	7^-	23.7(16)		11.2	
^{202}Pb	19^-	0.5(1)			0.02(1)
	16^+	2.7(3)			0.15(2)
	7^-	9.0(7)			17.3(2)
^{200}Pb	19^-	0.8(2)			0.07(2)
	12^+	14.2(7)			3.2(1)
	9^-	32.9(7)			12.5(3)
^{198}Pb	12^+	18.5(10)			6.2(2)
	7^-	45.1(12)			34.9(6)